Supplementary Information for:

The coil-to-globule transition of single-chain polymeric nanoparticles with a chiral internal secondary structure

Gijs M. ter Huurne,[†] Martijn A. J. Gillissen,[†] Anja R. A. Palmans,*[,†] Ilja K. Voets,*[,†] and E. W. Meijer[†]

[†]Institute for Complex Molecular Systems, Laboratory of Macromolecular and Organic Chemistry, Eindhoven University of Technology, P.O. Box 513, 5600 MB, Eindhoven, The Netherlands.

1. Instrumentation

^{1}H- and ^{13}C-NMR spectra were recorded on a Varian Gemini 400 MHz NMR (400 MHz for ^{1}H-NMR and 100 MHz for ^{13}C-NMR). The ^{1}H-NMR chemical shifts are reported in ppm downfield from tetramethylsilane (TMS). ^{13}C-NMR chemical shifts are reported downfield from TMS using the resonance of the deuterated solvent as internal standard. Abbreviations used are s = singlet, d = doublet, dd = double doublet, t = triplet, q = quartet and m = multiplet.

Infrared spectroscopy was measured using a PerkinElmer FT-IR Spectrum Two equipped with a Perkin-Elmer UATR Two.
Matrix assisted laser desorption/ ionization time of flight mass spectra (MALDI-TOF-MS) was acquired using a Bruker Autoflex Speed MALDI-TOF using α-cyano-4-hydroxycinnamic acid (CHCA) or *trans*-2-[3-(4-*tert*-butylphenyl)-2-methyl-2-propenylidene]malononitrile (DCTB) as matrices.

A DSC Q2000 under nitrogen atmosphere was used to determine the products thermal transitions. The second heating run was used to determine the transition with heating and cooling rates of 10 °C min^{-1}.

DMF-SEC measurements were performed on a PL-GPC-50 plus from Polymer Laboratories (Varian Inc. Company) with a refractive index detector. As elution, dimethylformamide containing 10 mM LiBr (flow = 1 mL min^{-1}) was used operating at 50 °C with a Shodex GPC-KD-804 column (exclusion limit = 400 000 Da; 0.8 cm i.d. × 300 mm) calibrated with polyethyleneoxide (Polymer Laboratories).

2. Materials

All commercial reagents were purchased from Aldrich and used as received unless stated otherwise. All solvents were purchased from Biosolve and the deuterated solvents were purchased from Cambridge Isotopes Laboratories. Jeffamine® M-1000 polyetheramine (**2**) was provided by Huntsman. *Cis*-5-norbornene-*exo*-2,3-dicarboxylic anhydride (**1**), [S1] *N*-Boc-1,12-dodecanediamine (**4**), [S2] 3,5-bis(3[3'-((*S*)-3,7-dimethyloctyoxy)benzoylamino)-2,2'-bipyridyl] aminocarbonyl)benzoic acid (**6**), [S3, S4, S5, S6] and the 3rd generation Grubbs catalyst – dichloro[1,3-bis (2,4,6-trimethylphenyl)-2-imidazolidinylidene](benzylidene)bis(pyridine)ruthenium(II) [S7] – were prepared according to literature procedures.

3. Monomer and polymer synthesis and characterization

Synthesis of Jeffamine monomer (3)

Cis-5-norbornene-*exo*-2,3-dicarboxylic anhydride (**1**) (2.67 g, 16.26 mmol) and Jeffamine® M-1000 polyetheramine (**2**) (14.94 g, 14.33 mmol) were dissolved in toluene (80 mL). The reaction mixture was refluxed overnight, after addition of triethylamine (2 mL, 14.3 mmol), using a Dean-Stark apparatus. Once ^{1}H-NMR indicated complete conversion, the solvent was removed under vacuum. The obtained product was purified by column chromatography (silica, ethanol : chloroform - 1 : 0 → 1 : 1). The purified product was dried using high vacuum, giving pure **3** in a 57 % yield (9.63 g, 8.10 mmol).

^{1}H-NMR (400 MHz, $CDCl_3$): δ 6.27 (s, 2H), 4.49 - 4.30 (m, 1H), 4.06 - 3.94 (m, 1H), 3.91 - 3.15 (m, 93H), 2.71 - 2.55 (m, 2H), 1.54 - 1.40 (m, 2H), 1.34 - 1.24 (m, 3H), 1.18 - 1.00 (m, 5H); ^{13}C-NMR (100 MHz, $CDCl_3$): δ 178.2, 137.9, 75.2, 74.6, 74.5, 73.3, 72.9, 72.8, 71.9, 70.6, 70.1, 68.4, 59.0, 47.5, 47.3, 46.7, 45.4, 42.7, 17.5, 17.3, 17.0, 14.1; FT-IR (ATR): ν (cm^{-1}) = 2866, 1767, 1698, 1456, 1394, 1371, 1349, 1326, 1289, 1250, 1206, 1096, 1039, 990, 947, 877, 849, 789, 773, 722, 698, 642, 585, 515; MALDI-TOF-MS: m/z found: broad range with maximum at: 1050.64; T_m = 29.3°C.

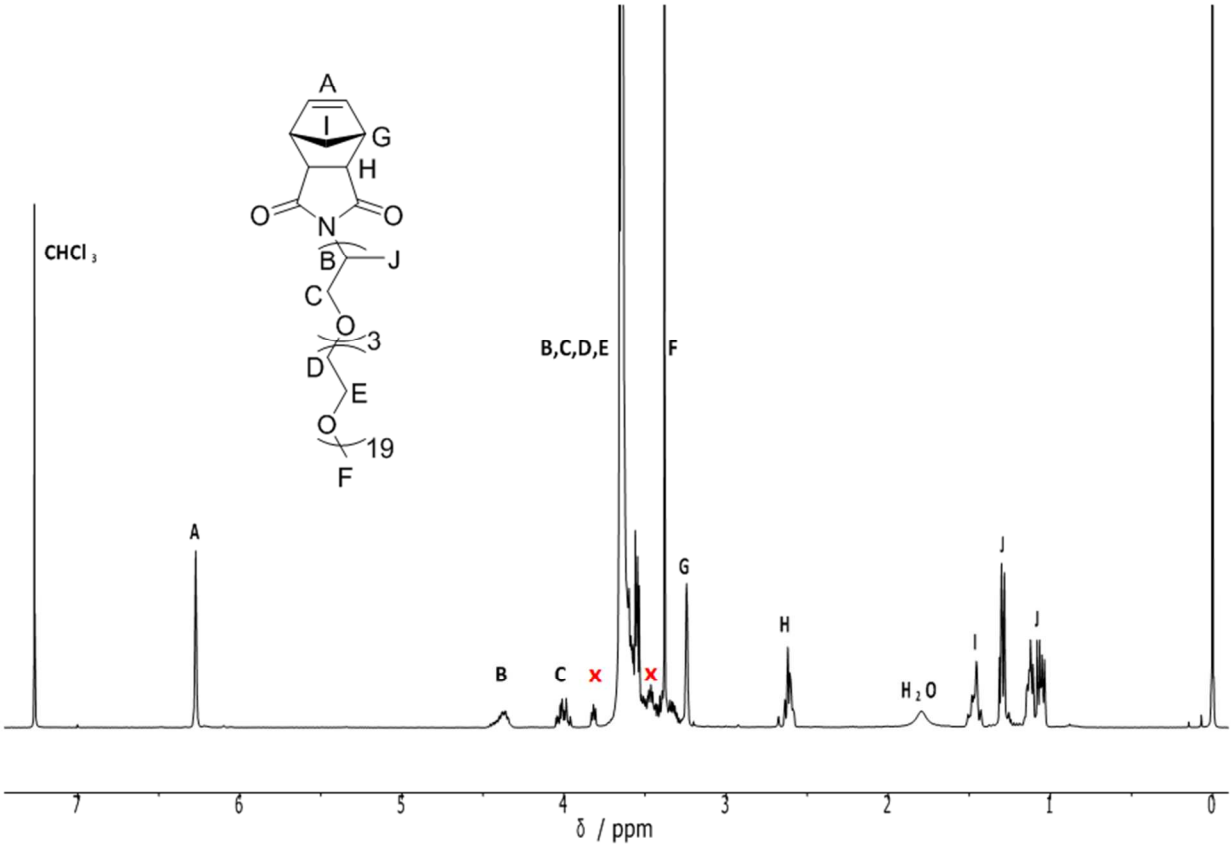

Figure S1: The ^{1}H-NMR spectrum of hydrophilic monomer **3** in $CDCl_3$.

Synthesis of the spacer monomer (5)

Cis-5-norbornene-*exo*-2,3-dicarboxylic anhydride (**1**) (1.00 g, 6.09 mmol) and *N*-Boc-1,12-dodecanediamine (**4**) (2.11 g, 7.02 mmol) were dissolved in toluene (50 mL). Triethylamine (1 mL, 7.2 mmol) was added to the mixture before it was refluxed overnight using a Dean-Stark apparatus. All solvents were removed using vacuum once ^{1}H-NMR indicated full conversion. The crude product was redissolved in chloroform (50 mL) and washed with a 10% citric acid (aq.) (3 × 20 mL). The mixture was subsequently washed with $NaHCO_3$ (sat.) (1 × 20 mL) and brine (1 × 20 mL) before it was dried over $MgSO_4$. After filtration the product was passed through a silica plug using 4 % methanol in chloroform as eluent. All volatiles were removed *in vacuo* giving pure **5** in a 92 % yield (2.50 g, 5.60 mmol).

^{1}H-NMR (400 MHz, $CDCl_3$): δ 6.29 (s, 2H), 4.56 (broad, 1H), 3.45 (t, J = 7.5 Hz, 2H), 3.27 (s, 2H), 3.10 (q, J = 8 Hz, 2H), 2.67 (s, 2H), 1.63 - 1.36 (m, 13H), 1.36 - 1.01 (m, 16H); ^{13}C-NMR (100 MHz, $CDCl_3$): δ 178.1, 156.0, 137.8, 78.9, 77.3, 47.8, 45.2, 42.7, 40.6, 38.7, 30.1, 29.5, 29.4, 29.3, 29.1, 28.4, 27.8, 26.9, 26.8; FT-IR (ATR): ν (cm^{-1}) = 3376, 2997, 2985, 2969, 2935, 2918, 2850, 1767, 1694, 1632, 1515, 1484, 1469, 1393, 1364, 1329, 1325, 1289, 1261, 1244, 1211, 1167, 1144, 1105, 1050, 1011, 996, 982, 938, 907, 890, 880, 870, 836, 814, 798, 779, 733, 723, 641, 609, 578, 537, 503, 481; MALDI-TOF-MS: m/z calc. : 446.6; found: 469.3 ($M + Na^+$); T_m = 71.3°C.

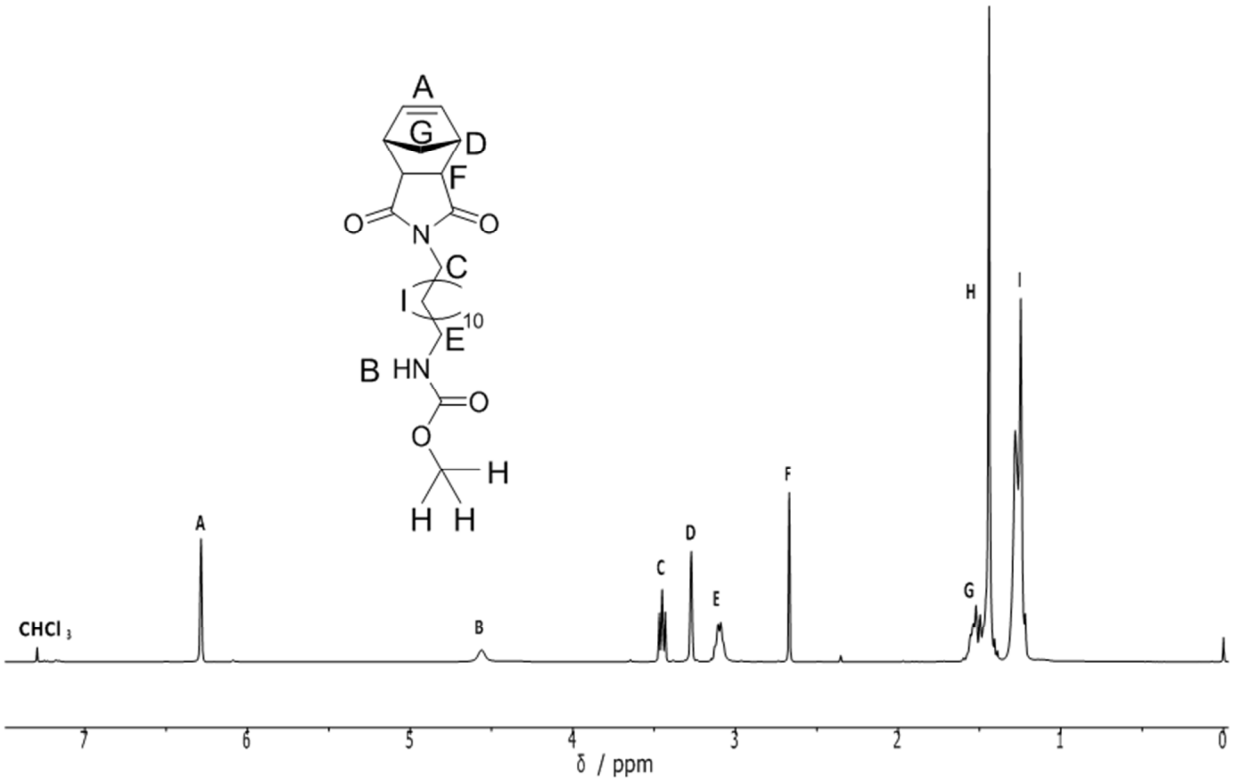

Figure S2: The ^{1}H-NMR spectrum of the Boc-protected linker monomer (**5**) in $CDCl_3$.

Synthesis of BiPy-BTA monomer (7)

To a solution of compound **5** (0.14g, 0.31 mmol) in dichloromethane (5 mL), trifluoroacetic acid (0.24 mL, 2.2 mmol) was added. The mixture was stirred for three hours until ^{1}H-NMR indicated full conversion to the corresponding TFA adduct, which was obtained via evaporation of all volatiles. The product was used without further purification.

Simultaneously the BiPy-BTA carboxylic acid (**6**) (0.50 g, 0.30 mmol) was suspended in dry dichloromethane (4 mL) under argon atmosphere. To this suspension, Ghosez's reagent - (1-Chloro-N,N,2-trimethyl-1-propenylamine) - (0.10 mL, 0.73 mmol) was added. The mixture was stirred until FT-IR suggested full conversion to the corresponding acid chloride, after which all solvents were evaporated. The product was used without further purification. FT-IR (ATR): ν (cm^{-1}) = 3048, 2954, 2928, 2870, 1758 (C=O acid chloride), 1640, 1568, 1514, 1493, 1468, 1443, 1427, 1397, 1371, 1328, 1295, 1264, 1239, 1191, 1178, 1100, 985, 800, 730, 699, 637, 596, 503.

The TFA adduct of **5** was dissolved in dry dichloromethane (5 mL) and added to a solution of the BiPy-BTA acid chloride in dichloromethane (5 mL) under an argon atmosphere. Once dissolved, triethylamine (0.3 mL, 2.15 mmol) was added and the mixture was stirred overnight. Once FT-IR indicated complete conversion, the crude product was precipitated by the addition of acetone (15 mL). The product was purified by column chromatography (silica, chloroform : ethylacetate - 1 : 0 → 4 : 1). The purified product was dried using high vacuum, giving pure **7** in a 79 % yield (0.45 g, 0.24 mmol).

^{1}H-NMR (400 MHz, $CDCl_3$): δ 15.48 (s, 2H), 14.38 (s, 2H), 9.51 (dd, J = 8.5 Hz, 1.5 Hz, 2H), 9.41 (dd, J = 8.5 Hz, 1.5 Hz, 2H), 9.16 (s, 1H), 9.00 (dd, J = 4.6 Hz, 1.5 Hz, 2H), 8.84 (s, 2H), 8.44 (dd, J = 4.6 Hz, 1.5 Hz, 2H), 7.56 (dd, J = 8.6 Hz, 4.6 Hz, 2H), 7.48 (dd, J = 8.5 Hz, 4.6 Hz, 2H), 7.29 (s, 4H), 6.55 (t, J = 5.6 Hz, 1H), 6.27 (s, 2H), 4.20 - 4.02 (m, 12H), 3.59 (q, J = 6.9 Hz, 2H), 3.45 (t, J = 8.0 Hz, 2H), 3.26 (s, 2H), 2.66 (s, 2H), 1.99 - 1.08 (m, 85H), 1.05 - 0.69 (m, 54H); ^{13}C-NMR (100 MHz, $CDCl_3$): δ 178.1, 166.3, 165.5, 164.1, 153.2, 142.2, 141.9, 141.3, 140.3, 137.8, 137.6, 137.4, 135.8, 135.6, 130.3, 129.9, 129.6, 129.0, 124.7, 124.0, 106.6, 77.2, 71.8, 67.9, 47.8, 45.2, 42.7, 40.6, 39.4, 39.3, 38.8, 37.5, 37.4, 37.4, 36.5, 29.9, 29.7, 29.5, 29.5, 29.5, 29.4, 29.4, 29.1, 28.0, 27.8, 27.1, 26.9, 24.8, 22.7, 22.7, 22.6, 22.6, 19.6, 19.6; FT-IR (ATR): ν (cm^{-1}) = 2953, 2925, 2869, 1769, 1699, 1669, 1567, 1515, 1493, 1467, 1443, 1427, 1371, 1328, 1298, 1237, 1200, 1171, 1114, 1073, 1041, 997, 952, 914, 863, 827, 797, 745, 729, 721, 664, 637, 589, 464; MALDI-TOF-MS: m/z calc. : 2020.9; found: 2021.5 (M + H^+), 2043.4 (M + Na^+), 2059.4 (M + K^+); $T_{Cr\text{-}LC}$ = 182.9°C, $T_{LC\text{-}I}$ = 199.4°C.

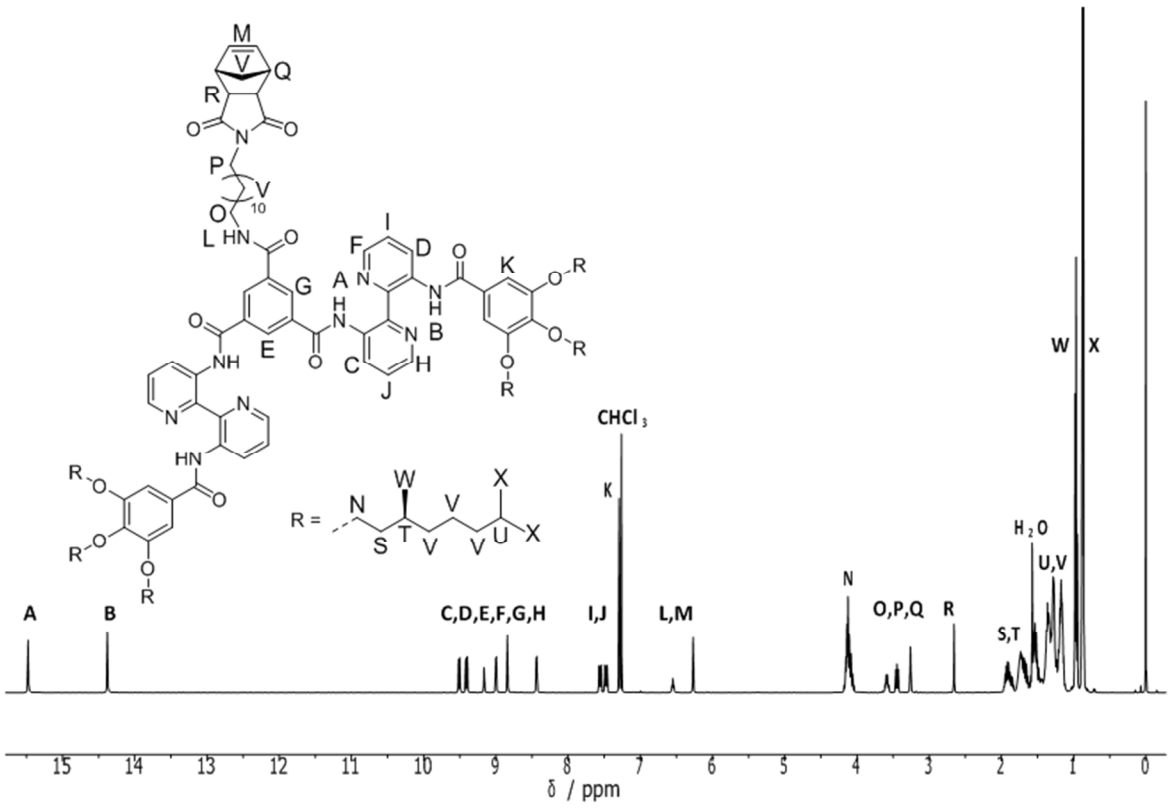

Figure S3: The ^{1}H-NMR spectrum of the pure BiPy-BTA monomer (**7**) in $CDCl_3$.

General synthetic procedure for the polymers

Dry tetrahydrofuran was degassed in a Schlenk tube by bubbling argon for at least half an hour. Subsequently the monomers were dissolved in the degassed tetrahydrofuran (2 mL) under argon atmosphere before being transferred to a Schlenk tube (at 30 °C) used for the polymerization. The 3rd generation Grubbs catalyst was dissolved in degassed tetrahydrofuran (20 µL) and added to the monomer solution (Table S2). The polymerizations were run for 30 minutes before being quenched via the addition of ethyl vinyl ether (1 mL). The mixture was stirred for another 30 minutes before the polymer solution was precipitated in a mixture of cold n-pentane and diethylether (1 : 1). The polymers were obtained by drying the precipitate.

p1-3: ^{1}H-NMR (400 MHz, $CDCl_3$): δ 5.91 – 5.24 (m, backbone *CH=CH*), 4.50 - 4.19 (m, Jeffamine® M-1000), 4.05 - 3.18 (m, Jeffamine® M-1000), 3.11 - 2.35 (m, polymer backbone), 2.35 - 1.98 (m, polymer backbone), 1.80 - 1.42 (m, polymer backbone), 1.42 - 1.20 (m, Jeffamine® M-1000), 1.20 - 0.94 (m, Jeffamine® M-1000); T_m = 30.5°C.

p4-9: ^{1}H-NMR (400 MHz, $CDCl_3$): δ 15.48 (s, 2H, intra. H-bond), 14.38 (s, 2H, intra. H-bond), 9.63 - 8.28 (arom. BiPy - BTA), 7.67 - 7.35 (arom. BiPy - BTA), 7.29 (s, 4H), 6.10 - 5.08 (m, backbone *CH=CH*), 4.54 - 4.19 (m, 12H, BiPy – BTA, OCH_2), 4.19 - 2.43 (m, Jeffamine® M-1000,

aliphatic spacer and polymer backbone), 2.43 - 0.56 (polymer backbone, aliphatic spacer and BiPy - BTA side chains); T_m = 29.7°C.

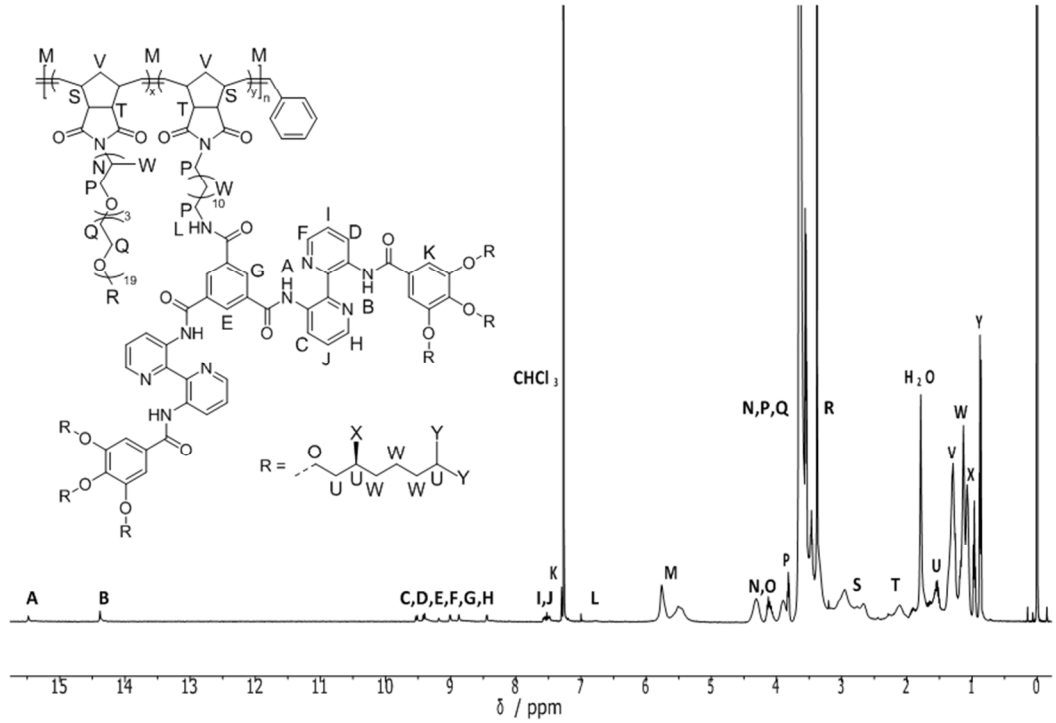

Figure S4: A typical ^{1}H-NMR spectrum for the functionalized polymers (**p4-9**) in $CDCl_3$.

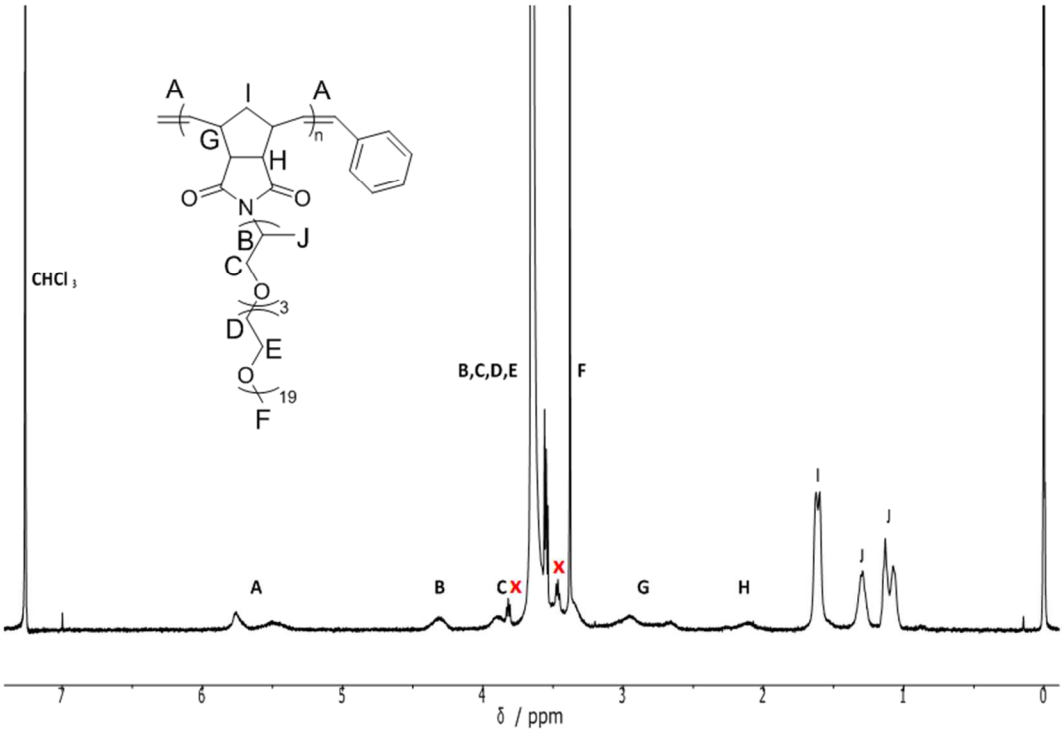

Figure S5: A typical ^{1}H-NMR spectrum for a reference polymer (**p7-p9**) in $CDCl_3$.

Table S1: Overview of the synthesized polymers with various BiPy-BTA incorporations and degrees of polymerization.

Polymer	Feed mol% **7** [%]	Conversion[a] [%]	Obs. mol% BiPy[a] [%]	DP^a [-]	$M_n{}^b$ [kDa]	$Đ_M{}^b$ [-]
p1 (p0%)	0	100	0	97	49.0	1.29
p2	0	100	0	197	63.2	1.38
p3	0	96	0	418	105.8	1.51
p4 (p5%)	5	100	4.9	94	44.7	1.23
p5	5	100	4.3	171	65.4	1.51
p6	5	94	5.3	420	128.8	1.72
p7 (p10%)	10	100	10.2	96	44.3	1.30
p8	10	100	9.6	196	60.9	1.49
p9	10	96	10.9	394	126.9	1.59

[a] Determined by ^{1}H-NMR, [b] Determined using SEC.

Table S2: The amounts of reactant and catalyst used for the synthesis of **p1-9**.

Polymer	**3** [mg]	**7** [mg]	m_{cat} [mg]	Yield [mg / %]
p1 (p0%)	106.5	-	0.67	71.7 / 67
p2	102.8	-	0.32	45.8 / 45
p3	99.7	-	0.14	56.5 / 57
p4 (p5%)	100.4	8.79	0.69	70.1 / 64
p5	104.9	9.03	0.39	80.0 / 70
p6	104.1	9.23	0.15	88.8 / 78
p7 (p10%)	100.3	17.77	0.71	82.6 / 70
p8	101.6	18.07	0.35	75.8 / 63
p9	102.7	18.06	0.17	56.7 / 47

4. Dynamic Light Scattering - Fitting procedure

Dynamic light scattering measurements were performed using a Malvern µV Zetasizer equipped with an 830 nm laser and a scattering angle of 90° at a temperature of 25 °C. Samples were prepared at 1 mg mL^{-1} and filtered with a 0.2 µm PVDF-filter (Whatman) in order to prevent the presence of dust. A fluorescence cell with a 1 cm path length was used for the measurement. The Origin 9.0 software package was used to simultaneously fit the obtained correlation functions with a tri-exponential decay function with shared parameters.

Light scattering experiments and literature indicated that THF/water mixtures and are not homogeneously mixed at a microscopic scale and small (R_H ≈ 0.3 – 1.0 nm) and large structures (R_H ≈ 200 – 600 nm) are present.[S8] Therefore, three different processes will be observed in DLS upon the inclusion of the single-chain polymeric nanoparticles, two processes related to the solvent mixture itself and one to the polymer particles. As observed, the diffusion coefficients for these three particle contributions are rather similar, resulting in correlation functions containing a shallow slope (Figure S6).

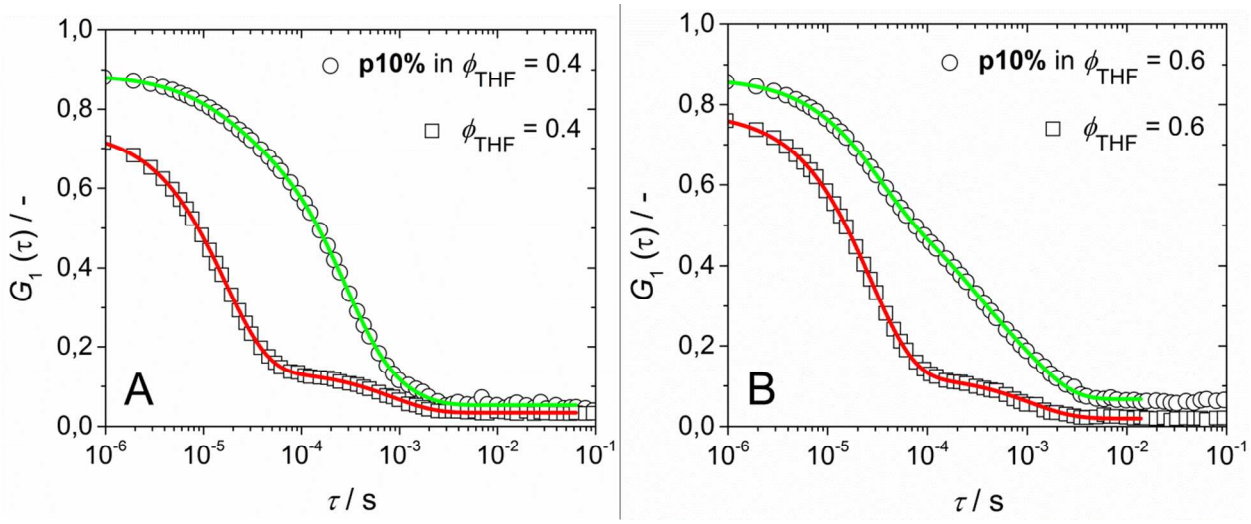

Figure S6: Two examples of the complex correlation functions of THF/water mixtures with and without **p10%**, fitted using a simultaneous tri-exponential fit (c = 1 mg mL^{-1}, 25 °C). A) **p10%** in ϕ_{THF} = 0.4; B) **p10%** in ϕ_{THF} = 0.6 THF.

A simultaneous fitting procedure with global parameters was used in order to extract the decay rate corresponding to the SCPN's diffusion. The correlation functions of the THF/water mixture in the presence and absence of the polymer, were therefore fitted with a tri-exponential decay function, defined by amplitudes (A, B, C), decay rates ($\Gamma_{1,2,3}$), correlation time (τ) and offset I_0 (Equation S1).

$$G_1(\tau) = A \cdot e^{(-\Gamma_1 \cdot \tau)} + B \cdot e^{(-\Gamma_2 \cdot \tau)} + C \cdot e^{(-\Gamma_3 \cdot \tau)} + I_0 \quad (S1)$$

The correlation function of the solvent mixture was fitted without the intermediate process (B = 0) because only the fast and slow processes are present. The solvent's decay rates corresponding to the fast and slow processes were assumed to be the same in the presence and absence of the polymers. Therefore, the correlation functions of the polymer solution and solvent mixture were fitted with global fast and slow decay rates ($\Gamma_{1,3}$), while letting the intermediate process (Γ_2), corresponding to the SCPN, free. As shown in Figure S6 excellent simultaneous fits were obtained via this approach. The decay rate corresponding to the single-chain polymeric nanoparticle was converted into its corresponding diffusion coefficient, and subsequently transformed into its hydrodynamic radius (R_H) via the Stokes-Einstein equation. The solvent's macroscopic properties, such as the refractive index and viscosity change with its composition. Therefore values for the refractive index and viscosity were obtained from literature.[S9]

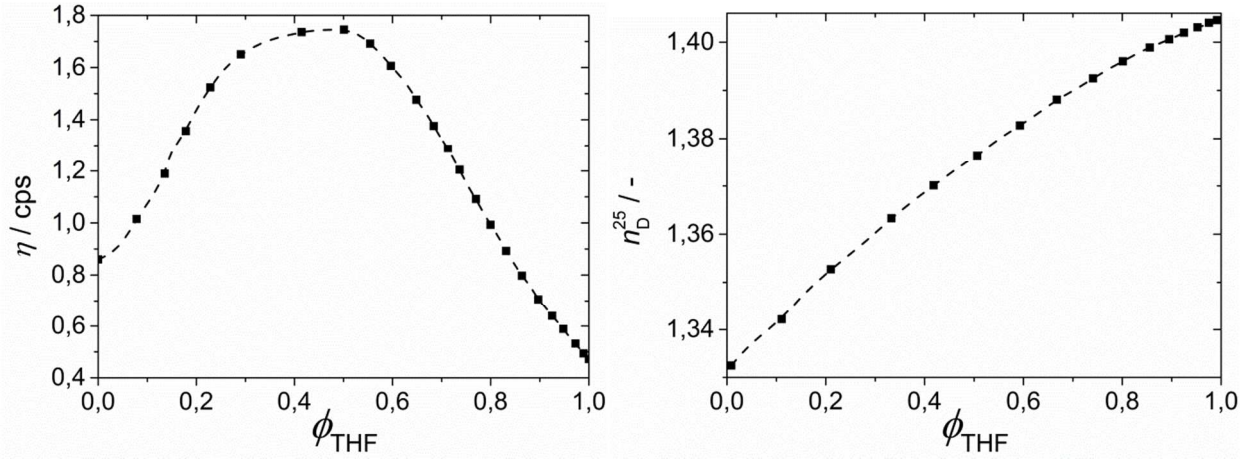

Figure S7: The viscosities and refractive indices for aqueous THF solutions at 25 °C.[S9]

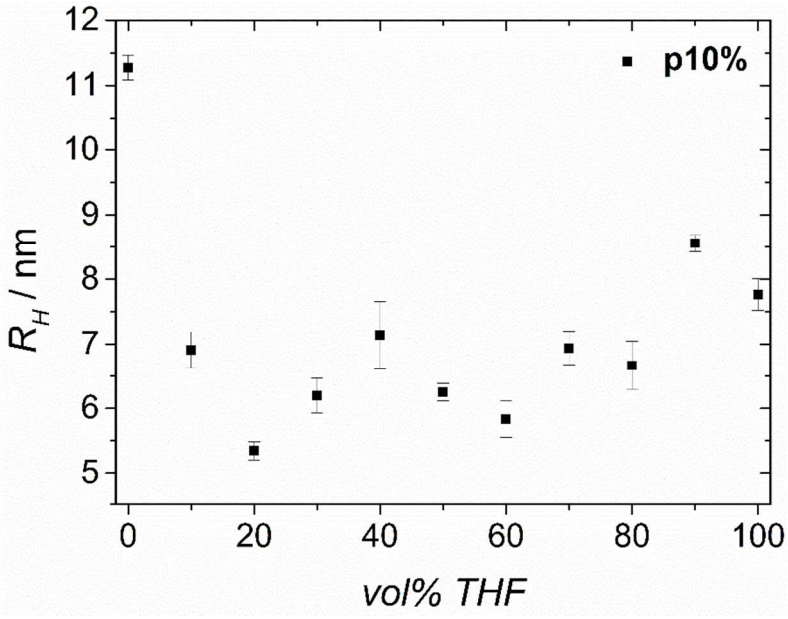

Figure S8: The effect of THF on the hydrodynamic radius (R_H) of **p10%.**

Table S3: The hydrodynamic radii (R_H) for **p10%** in various THF/water compositions.

ϕ_{THF}	R_H [nm]
0	11.3 ± 0.19
0.1	6.9 ± 0.28
0.2	5.3 ± 0.14
0.3	6.2 ± 0.26
0.4	7.1 ± 0.52
0.5	6.2 ± 0.14
0.6	5.8 ± 0.28
0.7	6.9 ± 0.25
0.8	6.7 ± 0.38
0.9	8.6 ± 0.13
1.0	7.8 ± 0.24

5. Temperature-dependent Circular Dichroism spectroscopy

UV/Vis and circular dichroism measurements were performed with a Jasco J-815 spectro polarimeter in combination with a PFD-425S/15 Peltier-type temperature controller. The molar circular dichroism $\Delta\varepsilon$ was calculated from $\Delta\varepsilon$ = CD effect / (32980 × c × l) in which c is the concentration and l is the optical pathway. Typical CD measurements were performed at 3×10^{-5} M and an optical pathway of 1 cm. The measurement at higher concentration (3×10^{-4} M) was performed using a pathway of 0.1 cm. The temperature-dependent CD measurements were performed by monitoring the magnitude of the CD effect ($\Delta\varepsilon$) at a single wavelength (λ = 386 nm) during heating and cooling. A cooling rate of 60 °C hr^{-1} was used over the required temperature regime.

The effect of the solvent composition

The effect of THF on the folding of the SCPNs was studied via temperature-dependent CD spectroscopy measurements on **p10%** in various THF/water compositions.

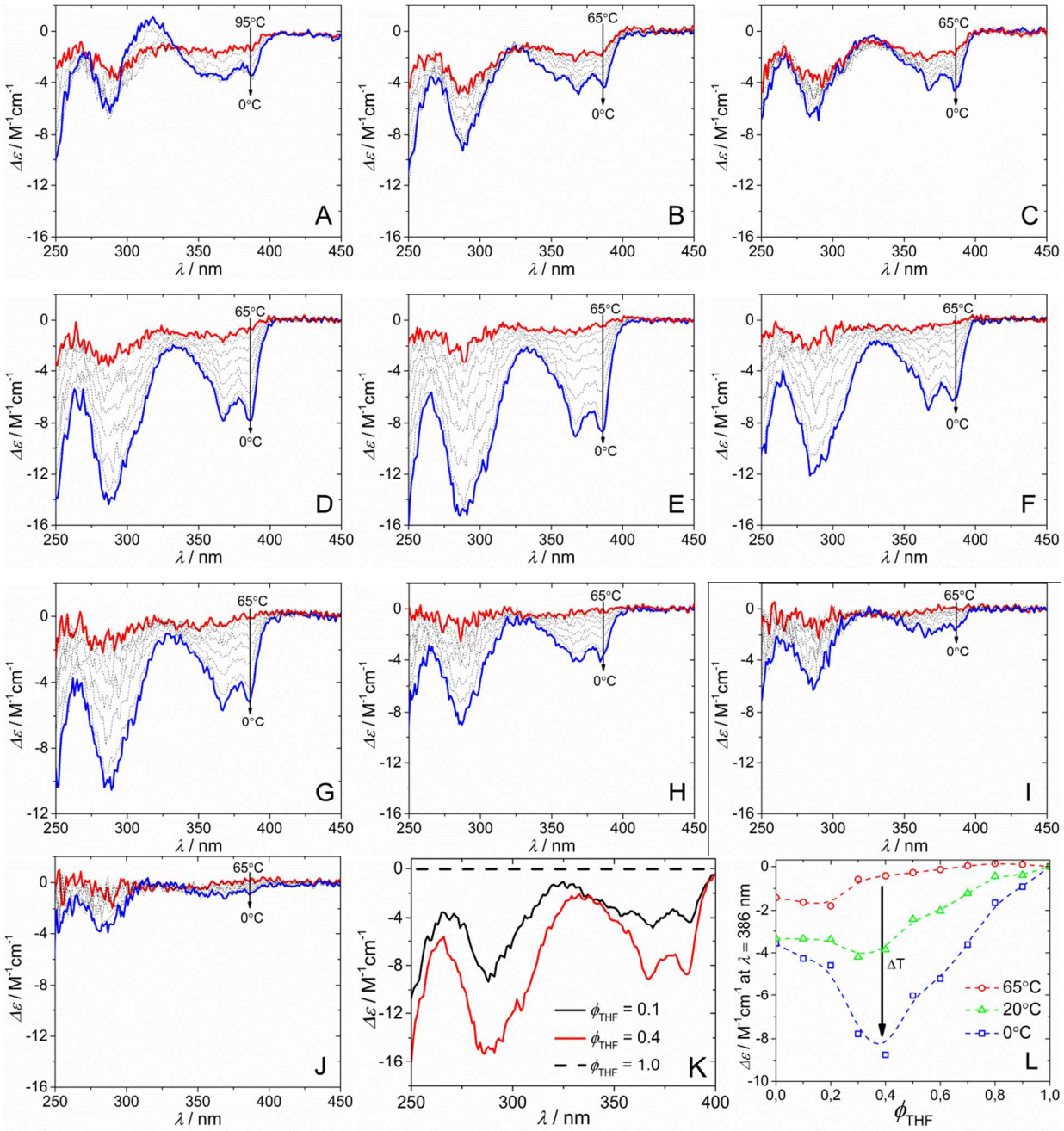

Figure S9: The CD spectra for **p10%** ($c_{BiPy\text{-}BTA}$ = 3 × 10^{-5} M) at various temperatures with ϕ_{THF} = ; A) 0.0; B) 0.1; C) 0.2; D) 0.3; E) 0.4; F) 0.5; G) 0.6; H) 0.7; I) 0.8; J) 0.9; K) the CD effects at various solvent ratios; L) the CD effect at 386 nm as a function of solvent composition and temperature.

Optimal folding

Overlapping cooling curves for the **p4-6** and **p7-9** solutions, with a constant BiPy-BTA concentration ($c_{\text{BiPy-BTA}}$ = 3 × 10^{-5} M), indicated that the degree of polymerization did not influence the polymer's folding behavior (Figure S10A). The folding is, however, clearly influenced by changes in the polymer's BiPy-BTA incorporation. An increase in disc incorporation results in a stronger CD effect. Remarkably, however, the CD effect is approximately two times stronger when the amount of BiPy-BTAs per chain is doubled. Furthermore, the polymer's folding proves to be independent of its concentration since the curves still overlap upon a tenfold increase in concentration (Figure S10B). This shows that folding is an intrachain process.

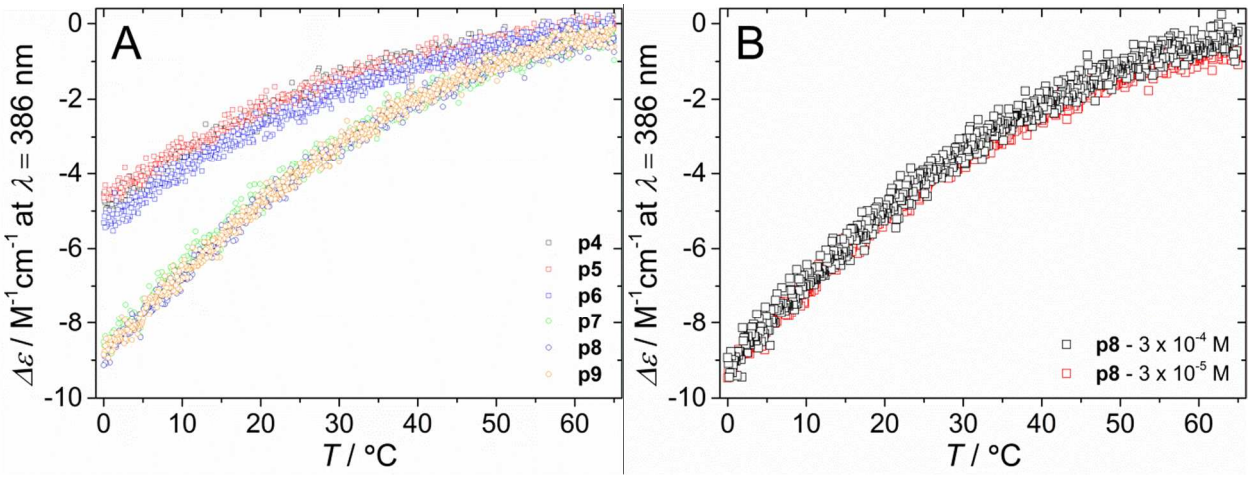

Figure S10: A) The cooling curves monitoring **p4-9**'s folding behaviour in ϕ_{THF} = 0.4 as a function of temperature (λ = 386 nm, $c_{\text{BiPy-BTA}}$ = 3 × 10^{-5} M); B) **p8** a two different concentrations (λ = 386 nm, $c_{\text{BiPy-BTA}}$ = 3 × 10^{-4} M and $c_{\text{BiPy-BTA}}$ = 3 × 10^{-5} M).

6. Small-angle X-ray Scattering

Small-angle X-ray scattering (SAXS) was performed on a SAXSLAB Ganesha system using a GeniX-Cu ultra-low divergence source producing X-ray photons with a wavelength of 1.54 Å and a flux of 1 x 10^8 ph s^{-1}. Scattering patterns were collected using a Pilatus 300K silicon pixel detector. Sample-to-detector distances of 0.13 and 1.53 m were used giving an observed q range of 1.3×10^{-3} $nm^{-1} \leq q \leq 2.4$ nm^{-1}. The solutions (typically 5 mg mL^{-1}) were measured in 2 mm quartz capillaries, typically measurement times were: 1 h at a sample-detector distance of 0.13 m, 5 h at 0.73 m and 9h at 1.53 m. The SAXSgui software package was used to radially averaged the resulting 2D images to obtain the intensity $I(q)$ vs. q profiles. Standard data reduction procedures, i.e. subtraction of the solvent's contribution, were performed using the same software. The curves were fitted using the SASfit 0.93.5 and SasView-2.2.0 software packages. Typically a generalized Gaussian coil model, representing the polymeric backbone, was used in combination with a sphere model, representing the short BiPy-BTA stacks, to fit the scattering curves.

The generalized Gaussian coil model

To model the self-avoiding polymer chain a generalized Gaussian coil model is used. This model contains three parameters: R_G, the radius of gyration, ν, the excluded volume parameter from the Flory mean field theory and I_0, the scattering intensity at $q = 0$. The used form factor describing the polymer is solution is: [S10, S11]

$$I_{\mathrm{gGc}}(q) = I_0 \frac{U^{\frac{1}{2\nu}}\Gamma\left(\frac{1}{2\nu}\right) - \Gamma\left(\frac{1}{\nu}\right) - U^{\frac{1}{2\nu}}\Gamma\left(\frac{1}{2\nu}, U\right) + \Gamma\left(\frac{1}{\nu}, U\right)}{\nu U^{\frac{1}{\nu}}} \quad \text{(S2)}$$

$$U = (2\nu + 1)(2\nu + 2)\frac{q^2 R_G^2}{6} \quad \text{(S3)}$$

$$\Gamma(a, x) = \int_x^\infty t^{a-1} e^{-t} dt \quad \text{(S4)}$$

$$\Gamma(a) = \Gamma(a, 0) = \int_0^\infty t^{a-1} e^{-t} dt \quad \text{(S5)}$$

Typical value for the solvent quality parameter ν, are:

- $\nu = 1/3$: Bad solvent
- $\nu = 1/2$: Θ-solvent
- $\nu = 3/5$: Good solvent

The sphere model

The small features related to the BiPy-BTAs are modelled with a sphere model containing two parameters: R, being its radius and $\Delta\eta$, the scattering length density difference between particle and matrix. [S10]

$$I_{\text{sphere}}(q,R) = K^2(q,R,\Delta\eta) \quad \text{(S6)}$$

$$K(q,R,\Delta\eta) = \frac{4}{3}\pi \cdot R^3 \Delta\eta \cdot 3\frac{\sin(qR) - (qR)\cos(qR)}{(qR)^3} \quad \text{(S7)}$$

$$\lim_{q=0} I_{\text{sphere}}(q,R) = (\frac{4}{3}\pi R^3 \Delta\eta)^2 \quad \text{(S8)}$$

The effect of disc incorporation

The effect of the disc incorporation on the SCPN's structure and shape was studied by comparing polymers with similar lengths (*DP* ≈ 100) but different BiPy-BTA incorporations (**p0%**, **p5%** and **p10%**). All these experiments were performed in the 'optimal' solvent composition (ϕ_{THF} = 0.4). The obtained curves were fitted using the just described combined Gaussian coil and sphere model with a fixed sphere radius of 1.1 nm.

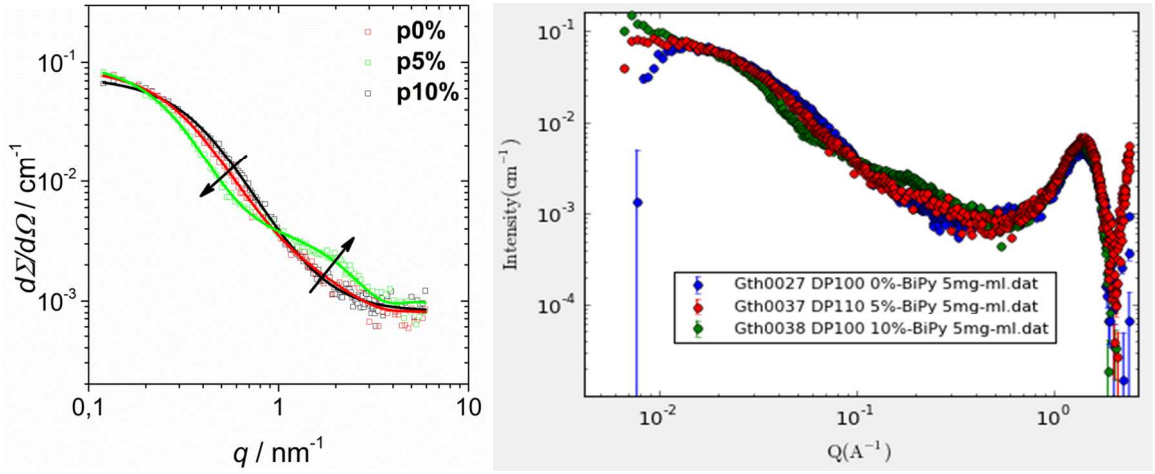

Figure S11: Left: the plotted curves for **p0%**, **p5%** and **p10%** fitted with the combined Gaussian coil and fixed radius sphere model (5 mg mL^{-1}, 20 °C). Right: the original SAXS curves for the same polymers.

Table S4: The data corresponding to the fitted SAXS curves of polymers **p0%**, **p5%** and **p10%**.

BiPy-BTA [%]	Polymer	R_G [nm]	± [nm]	ν [-]	± [-]	R_{sphere} [nm]	$\Delta\eta$ [cm^{-2}]	± [cm^{-2}]	R_H [nm]	ρ [-]
0	**p0%**	4.9	2.3×10^{-3}	0.36	1.4×10^{-4}	-	-	-	8.4 ± 0.26	0.6
5	**p5%**	5.9	4.5×10^{-3}	0.36	4.2×10^{-4}	1.1	5.4×10^{-6}	1.7×10^{-8}	6.5 ± 0.38	0.9
10	**p10%**	7.1	4.2×10^{-3}	0.26	2.7×10^{-4}	1.1	1.0×10^{-5}	4.3×10^{-9}	7.1 ± 0.52	1.0

The effect of solvent composition

The effect of solvent composition was investigated with SAXS by studying **p10%** in various solvent compositions (ϕ_{THF} = 0.1, 0.4 and 1.0) using SAXS. It was necessary to use ϕ_{THF} = 0.1 instead of pure water, as it proved to be nearly impossible to obtain the desired polymer concentrations in pure water. The combined Gaussian coil and sphere model, with a fixed sphere radius of 1.1 nm, was used to fit the obtained scattering profiles.

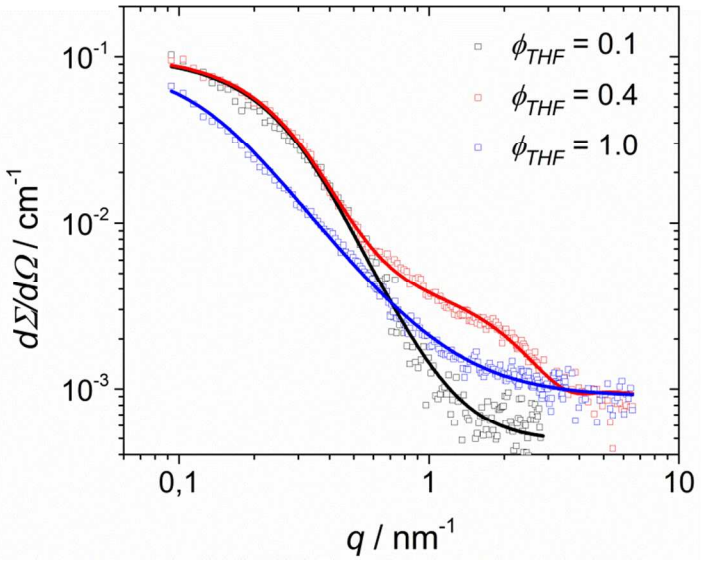

Figure S12: The data corresponding to the fitted SAXS curves of polymer **p10%** in various ϕ_{THF}.

Table S5: The data corresponding to the fitted SAXS curves of polymer **p10%** in various ϕ_{THF}.

ϕ_{THF}	R_G [nm]	± [nm]	ν [-]	± [-]	R_{sphere} [nm]	$\Delta\eta$ [cm^{-2}]	± [cm^{-2}]	R_H [nm]	ρ [-]
0.1	7.0	1.3×10^{-3}	0.31	1.4×10^{-4}	-	-	-	6.9 ± 0.28	1.0
0.4	7.1	4.0×10^{-3}	0.26	2.7×10^{-4}	1.1	1.0×10^{-5}	4.3×10^{-9}	7.1 ± 0.52	1.0
1.0	>10	-	0.47	2.4×10^{-4}	-	-	-	7.8 ± 0.24	>1.23

7. References

S1. Craig, D. *J. Am. Chem. Soc.* **1951,** 73, (10), 4889-4892.

S2. Cinelli, M. A.; Cordero, B.; Dexheimer, T. S.; Pommier, Y.; Cushman, M. *Bioorg. Med. Chem.* **2009,** 17, (20), 7145-7155.

S3. Palmans, A. R. A.; Vekemans, J. A. J. M.; Fischer, H.; Hikmet, R. A.; Meijer, E. W. *Chem. Eur. J.* **1997,** 3, (2), 300-307.

S4. Palmans, A. R. A.; Vekemans, J. A. J. M.; Havinga, E. E.; Meijer, E. W. *Angew. Chem. Int. Ed.* **1997,** 36, (23), 2648-2651.

S5. van Gorp, J. J.; Vekemans, J. A. J. M.; Meijer, E. W. *J. Am. Chem. Soc.* **2002,** 124, (49), 14759-14769.

S6. Roosma, J.; Mes, T.; Leclère, P.; Palmans, A. R. A.; Meijer, E. W. *J. Am. Chem. Soc.* **2008,** 130, (4), 1120-1121.

S7. Love, J. A.; Morgan, J. P.; Trnka, T. M.; Grubbs, R. H. *Angew. Chem. Int. Ed.* **2002,** 41, (21), 4035-4037.

S8. Yang, C.; Li, W.; Wu, C. *J. Phys. Chem. B* **2004,** 108, (31), 11866-11870.

S9. Hayduk, W.; Laudie, H.; Smith, O. H. *J. Chem. Eng. Data* **1973,** 18, (4), 373-376.

S10. Kohlbrecher, J. SASfit: A program for fitting simple structural models to small angle scattering data. https://kur.web.psi.ch/sans1/SANSSoft/sasfit.pdf

S11. Hammouda, B. Probing nanoscale structures - The SANS toolbox. http://www.ncnr.nist.gov/staff/hammouda/the_SANS_toolbox.pdf